A 2D and 3D Analysis on Electromagnetic Parameters of Spoke-shape Interior Permanent Magnet Synchronous Motor Using FEM

Supriya Naik[1], Baidyanath Bag[1], Kandasamy Chandrasekaran[1*]

[1] Department of Electrical Engineering, National Institute of Technology, Great Eastern Road, 492010 Chhattisgarh, Raipur, India
* Corresponding author, e-mail: kchandrasekaran.ee@nitrr.ac.in

Abstract

In industry, the most frequently used motors are induction motors (IMs), reluctance motors, and permanent magnet synchronous machines (PMSMs). Nowadays because of higher efficiency with higher power density, PMSM attracts its uses in every field of application. Hence, a spoke shape interior PM-based synchronous motor (IPMSM) with distributed winding is considered to discuss in this paper. Also, there has always been a dispute between 2D and 3D analysis of electromagnetic parameters of machines. Therefore, this paper discusses the accuracy, advantages, and difficulty level of 2D and 3D FEM analysis of the IPM motor model by considering several electromagnetic with electromechanical parameters such as torque, flux linkage, eddy current loss, etc. The performance of five different core materials is also considered for comparison. These analyses are carried out by using ANSYS Maxwell software. Spoke shape IPMSM of 0.55 kW with 220 V, 50 Hz is considered for analysis. The 2D and 3D comparison results of parameters under magnetostatic and transient conditions are presented and verified with the results reported in the literature. 2D FEM analysis has given more value in case of torque, stator current, and magnetic flux density than 3D analysis where as 3D analysis is give good performance for flux linkage, back EMF, and eddy current losses. Significant percentage changes with respect to observed materials in the results of 2D and 3D cases are reported. Silicon Steel M36 suitability for stator and rotor core is also observed. This 2D and 3D FEM analysis clarifies accuracy prior to design motor.

Keywords

2D-3D analysis, electromagnetic parameters, electromechanical parameters, finite element method, interior permanent magnet synchronous motor

1 Introduction

Industry trends and consumer expectations require modifying the size of electric motors to improve efficiency, reduce operating costs and increase life expectancy. A permanent magnet synchronous motor (PMSM) is one of the motors, which fulfilled the aforementioned features as defined in [1]. The presence of rare-earth permanent magnets enhances the demand for PMSM. It is the main reason behind the higher air gap magnetic flux density, higher power and torque density, and high efficiency of PMSM as compared to conventionally used IMs and reluctance motors. Due to the numerous benefits offered by PMSM, it is becoming imperative to conduct research in-depth analysis to improve the already available state-of-the-art. To extract the high performance of PMSM drive, day by day

many control strategies are developed [2, 3]. To improve performances, PMSM is available in two designs:

1. surface-mounted permanent magnet (SPM) motors;
2. interior permanent magnet (IPM) motors based on rotor designs [4].

Because the magnets are adherently connected to the rotor surface with the help of sleeve materials, SPM machines are considerably easier to manufacture as explained in [5]. Also, it has simple rotor structure and position controllability. Based on the performance in wider speed applications, the IPM machine is preferable as compared to SPM. IPM also has more efficiency, but equivalent magnetic circuit analysis can be complicated [6]. To make it easier for

understanding, an IPM motor with a spoke shape designed rotor is considered in this study. Designing of IPM has been improved mainly by the application of cost-effective optimization techniques with multi objectives.

The accurate motor's performance parameters estimation with its electromagnetic field analysis is an important stage for the overall computer-aided design modeling. To emphasize this, the electromagnetic analysis of the reluctance motor is described in [7]. Many approaches related to magnetic equivalent circuits have been developed for parameter verification. Optimization techniques with embedded numerical methods increase the complexity of the solving process. In [8], after the application of the optimization algorithm, 2D and 3D analyses were performed to verify the result and optimized the rotor skewing of the switched reluctance motor. Hence, in place of following the numerical methods, it should be easy to apply 2D and 3D analysis for verifying the design parameters. Many applications involve 2D and 3D both analyses to justify the quality of results. In [9], to observe the velocity skin effect on electromagnetic launchers, 2D and 3D finite element methods (FEM) is utilized. Similarly, observation of the quasi 3D model of IMs was performed in [10]. Thermal analysis of IMs was also observed through it [11]. A PMSM comparative analysis of 2D and 3D finite element method (FEM) is reported in [12] as an attractive alternative. Advanced designs of IMs (slotted solid rotor axial flux induction motors) are analyzed through 2D and 3D FEM methods [13]. When IPMSM is analyzed in 2D, it is commonly assumed that the error in performance evaluation is considerable for the smallest machine, as opposed to 3D analysis [14]. Ideally, a designer should be able to come up with a result as quickly as in 2D, but as accurately as in 3D. However, this statement lacks any real proof other than knowing the level of the error caused by the 2D analysis. The objective of this study was therefore to get a more reliable response to this question by conducting electromagnetic FEM analyses of a selected IPMSM in 2D and 3D while comparing the results. In [15] 2D and 3D analyses are considered for theoretical and experimental verification of synchronous homo-polar motors, which have been widely used in the era of traction. To reduce the timing of the experiment with the cost of testing, motors of every field are now verified through this novel 2D and 3D FEM analysis. The effect of the skew rotor with harmonic in electromagnetic parameters of IMs is discussed using 2D-3D model analysis in [16]. Different torque characteristics are also discussed for arc-linear flux switching

permanent-magnet motor using 2D and 3D FEM models [17]. In [18] 2D and 3D FEM analysis is applied for switched reluctance motor to show motor dynamic with the end coil effect. Its attractive property for traction application requires its proper analysis [19], but excessive-acoustic noise and low-power factors are some of the significant challenges. To avoid those issues PMSM motor comes into the scenario.

Among PMSM, IPMSM is mostly preferred for high with wider speed applications. But no literature focus on 2D and 3D magnetic circuit with details analysis of spoke-shape IPM motor. The spoke shape IPM motor requires less amount of PM as compared to other topologies, which results into a light weight, less cost, and small size. Due to light weight and small size, its demand increases in the field of light hybrid electric vehicle (EV). This also becomes an environmental friendly [20]. Therefore, a spoke shape IPM motor is considered for observation. In this condition, it is very important to know the flux density distribution in the airgap region between stator and rotor with various components along different directions like radial and tangential. Along with this, the radial force due to the radial component of airgap flux density also plays a great part in machine analysis. In addition to the value of this parameter, many other magnetic and electromechanical quantities will be affected, including the output torque, ripple factor in it, as well as the magnetic field distribution over the different motor parts (stator, rotor, and airgap), which in turn affects the motor's performance. So in the market now integrated software are available for 2D and 3D analysis of magnetic field in electromagnetic devices such as COMSOL Multi-Physics, MagNet, Infolytica, Maxwell Ansoft, Emag, ANSYS, FLUX, CEDRAT Software, MEGA, Bath University, Integrated Engineering Software, FEMM [21]. To show a comparative study between 2D and 3D analysis, output torque, flux linkage, and flux density of airgap etc. are considered. The percentage error between 2D and 3D measurements of each parameter of the IPM motor is calculated. They are helpful for the design engineer to take decisions that results an efficient motor within less time-period.

This paper focused on the 2D and 3D model FEM analysis of spoke shape IPM motor to understand the conflicts produced in analysis with the emersion of the core material. IPM motor is considered here due to its simple structure with higher efficiency compared to other types of PMSM motor. Except this, the spoke type of rotor structure motor has high torque due to its high reluctance torque, and concentrated flux density from the PM. It has

also irreversible demagnetization characteristics unlike conventional structures [22]. This study clarifies the accuracy of all electromechanical, and electromagnetic parameters for 2D and 3D models, and their comparative analyses are reported. The problem definition is elaborated in Section 2. Basic modelling of IPMSM in ANSYS Maxwell with the FEM and its details procedure in 2D and 3D Maxwell analysis are described in Section 3. All the derived result of different parameter and provides a comparative study is given in Section 4. Finally, the conclusion regarding all analyses observed from different parameter characteristics is reported in Section 5.

2 Description of the problem

To analyze transient and magnetostatic behavior of IPMSM, a balanced three-phase winding with coils coiled around the teeth of the stator with spoke shaped PMs in the inter surface of the rotor as shown in Fig. 1 is adapted from [23]. Spoke shape is easy constructability also provides good magnetic field with less amount of magnet [24, 25]. The three-phase stator windings exciting voltage are given as:

$$V_a = V_m \sin(\omega t + \theta), \tag{1}$$

$$V_b = V_m \sin(\omega t + \theta + 120^0), \tag{2}$$

$$V_c = V_m \sin(\omega t + \theta - 120^0). \tag{3}$$

An inner rotor approach is used here in a 4-pole, three-phase PMSM. A full-pitch distributed lap winding is employed on the stator, which has 24 slots. The outer diameter of the Stator's and rotor's core is 120 mm and 75 mm respectively. The active length of motor is 65 mm. The length of airgap between the stator and rotor core has been chosen to be 0.5 mm. Fig. 1(a) depicts a cross-sectional overall image of the IPMSM under investigation, as well as essential geometrical parameters. It represents a detailing of the stator slots as shown in Fig. 1(b).
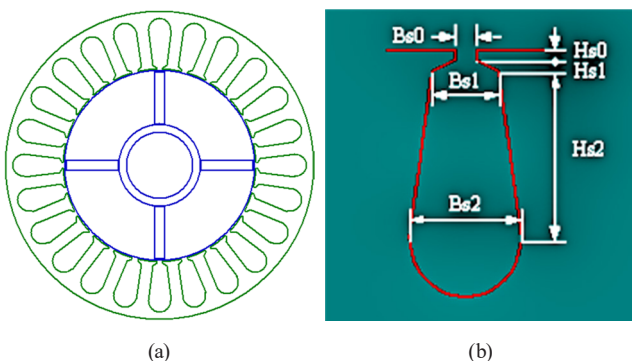

Fig. 1 IPMSM's assembly; (a) Cross section; (b) Detailed stator slots geometry [23]

Tables 1 to 3 illustrate the abovementioned quantities as well as the motor's attributes.

Table 1 summarizes the ratings of the corresponding IPM motors. The stator designing parameters are listed in Table 2.

The designing parameters of the rotor section are depicted in Table 3. The rotor is composed of four alternately poled and radially magnetized neodymium permanent magnets (NdFeB35).

Table 1 Parameters of the 0.55 kW IPMSM

Parameters	Value
Output power (W)	550
Output torque (Nm)	3.01
Line voltage rating (V)	220
Stator resistance (Ω)	2.16
Synchronous speed (rpm)	1500
Frequency (Hz)	50
RMS current per phase (A)	1.6
Peak current per phase (A)	2.4
Relative permeability of NdFeB35	1.099
Magnet width (mm)	3.5

Table 2 Designing parameters for stator core and slot of IPMSM

Quantity	Value
Outer diameter of stator (d_{out})	120 mm
Inner diameter of stator (d_{in})	75 mm
Active length of stator (L_{stat})	65 mm
Number of slots in stator (q)	24 mm
Opening width of slot (b_{ss0})	2.5 mm
Top width of slot (b_{ss1})	5.6 mm
Base width of slot (b_{ss2})	7.6 mm
Width of stator teeth (b_{st})	4.7 mm
Height of stator's slot (h_{ss})	13.5 mm
Tooth tip height in stator (h_{sw})	1.5 mm
Yoke height of stator (h_{sy})	9 mm
No. of conductors/slot (N)	58 mm
Wire diameter (D_{cond})	0.9116 mm
Wire area (A_{cond})	0.6527 mm^2

Table 3 Details of rotor core and permanent magnets in IPMSM

Quantity	Value
Number of permanent magnets (n)	4
Rotor's outer diameter (d_r)	74 mm
Diameter of shaft (d_{axis})	26 mm
Rotor's active length (L_{rot})	65 mm
Height of permanent magnet (l_m)	3.5 mm
Length permanent magnet (l_l)	18 mm
Airgap length (l_g)	0.5 mm
Pole arc/pole pitch ratio (2a)	65

Because of higher magnetic strength, NdFeB35 is mostly the preferred permanent magnet. These magnets are made from materials of higher energy density that can operate up to 150 °C. In this study, the temperature considered for motor operation is 75 °C.

2.1 Mathematical formulation of electromagnetic parameters

Maxwell's equations are the base for governing magnetic field analysis of IPMSMs in terms of mathematical background and equations. In order to measure the operational characteristics of IPMSMs, it is essential to resolve these Maxwell's equations as expressed in Eqs. (4)–(7) [12]:

$$\vec{\nabla} \times \vec{H} = J, \tag{4}$$

$$\vec{\nabla} \times \vec{E} = -\partial \vec{B}/\partial t, \tag{5}$$

$$\vec{\nabla} \times \vec{D} = \rho, \tag{6}$$

$$\vec{\nabla} \times \vec{B} = 0. \tag{7}$$

Here $\vec{H}$ represents the magnetic field vector, J defines the current density, $\vec{E}$ indicates the vector of the electric field, $\vec{B}$ defines the magnetic flux density vector, $\vec{D}$ represents the electric displacement vector, ρ denotes the electric charge density and t defines the time. The flux density is calculated by modifying these Maxwell's equations according to the coordinate system given in Eq. (8):

$$\frac{\partial}{\partial x}\left(\frac{1}{\mu}\frac{\partial \vec{A}}{\partial x}\right) + \frac{\partial}{\partial y}\left(\frac{1}{\mu}\frac{\partial \vec{A}}{\partial y}\right) = -J. \tag{8}$$

Here $\vec{A}$ is the magnetic vector potential and J is the current density, which is equal to zero for steel and air parts. The magnetic flux density components, B_x and B_y in the x and y axis directions are stated in Eqs. (9) and (10):

$$B_x = \frac{\partial \vec{A}}{\partial y}, \tag{9}$$

$$B_y = \frac{\partial \vec{A}}{\partial x}. \tag{10}$$

The magnetic flux density B is calculated as mentioned in Eq. (11):

$$B = \sqrt{B_x^2 + B_y^2}. \tag{11}$$

Similarly, for 3D model has been performed using Eq. (12):

$$\frac{\partial}{\partial x}\left(\frac{1}{\mu}\frac{\partial \vec{A}}{\partial x}\right) + \frac{\partial}{\partial y}\left(\frac{1}{\mu}\frac{\partial \vec{A}}{\partial y}\right) + \frac{\partial}{\partial z}\left(\frac{1}{\mu}\frac{\partial \vec{A}}{\partial z}\right) = -J. \tag{12}$$

Total magnetic flux density is determined (Eq. (13)):

$$B = \sqrt{B_x^2 + B_y^2 + B_z^2}. \tag{13}$$

Solving Maxwell's equations is required for finding magnetic forces and torque using finite-element method. A frequently used integration of Maxwell's stress tensor expression as given in Eq. (14) is used in the study:

$$\oint_s \vec{r} \times \vec{\sigma} \times dS = \oint_s \vec{r} \times \left[\frac{1}{\mu_0}\left(\vec{B} \times \hat{n}\right)\vec{B} - \frac{1}{2\mu_0}\vec{B}^2 \times \hat{n}\right] \times ds. \tag{14}$$

Here $\vec{\sigma}$ defines Maxwell's stress tensor, $\hat{n}$ represents unit normal vector of the interaction surface, $\vec{B}$ defines magnetic flux density vector, and r denotes the unit vector of r coordinate of the cylindrical coordinate system.

FEM is used to model and analyse 2D and 3D electromagnetics using 2D and 3D electromagnetic models, determining core losses, winding inductance, flux linkage, induced voltages, flux density, and eddy current losses.

3 Finite element modeling

Finite element method is effective at calculating local geometric details as well as the effects of ampere-conductor distributions and magnetization patterns. Fig. 2 elaborates the process of modelling in ANSYS MAXWELL [26]. It begins with the development of a model that is the right size and integrates material properties as an input. After that, the meshing of the matching model occurs. The number of tetrahedral elements is determined by mesh size. This number is also responsible for the accuracy of the results. Fig. 3(a) and (b) shows the 2D and 3D model of IPM motor having different stator core, conductors, rotor, PM with their corresponding material properties. Here, one fourth symmetry of simulation model is considered to reduce the computational time. NVIDIA 1660 Ti system is taken to carried out all the 2D and 3D finite element analysis (FEA) in ANSYS Maxwell 2018.1 version [27].

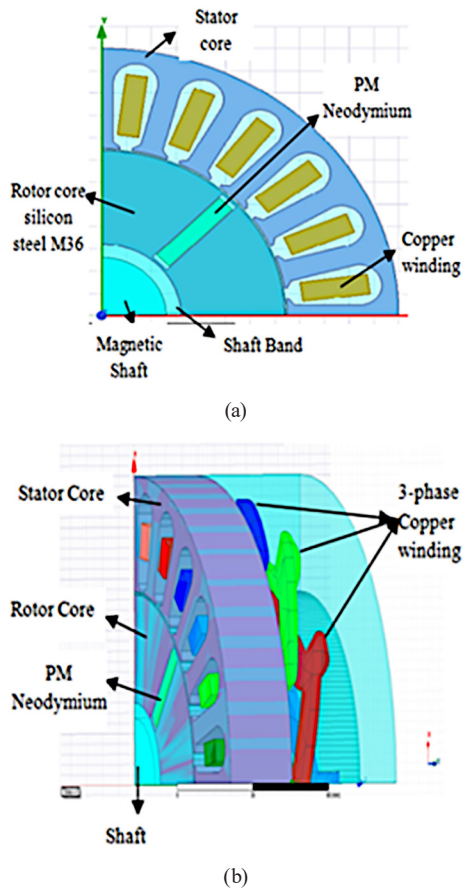
Fig. 2 Procedure of IPMSM model designing

Fig. 3 Modelling of IPMSM under; (a) 2D model; (b) 3D model

Fig. 4 IPMSM meshing formation; (a) 2D model; (b) 3D model

Table 4 Meshing and occupied memory details of an IPMSM with 2D and 3D analysis

Analysis	Total number of finite elements	Total space (MB)
2D	4102	65.3
3D	39656	634

In FEM, meshing formulation is carried after design with material properties and setting. In this, whole model is divided into many elements and nodes. The generated mesh for 2D and 3D analysis is depicted in Fig. 4(a) and (b). In both cases, numbers of element are different. After meshing formulation, 4102 and 39656 number of tetrahedral elements are considered for 2D and 3D analysis. Number of element size and nodes are deciding the memory space of model for solving. Memory details of both analyses are given in Table 4. From the Table 4 data it is clear that, 3D analysis takes more simulation time, and its details are given in Section 4.

Simulation is begins once meshing formulation completed and the solution is estimated. Airgap flux density is an important parameter that depends on the size of magnet and rotor topology. It helps to estimate the PMSM size. Motor output power with its torque is highly affected by this flux density.

4 2D and 3D model results and analysis using ANSYS
For the analysis of 2D and 3D model performance, a 0.55 kW, 1500 RPM, 3 phase, 4 poles IPM synchronous motor is taken. The stator and rotor outer radius considered are 120 and 74 mm respectively with same active length
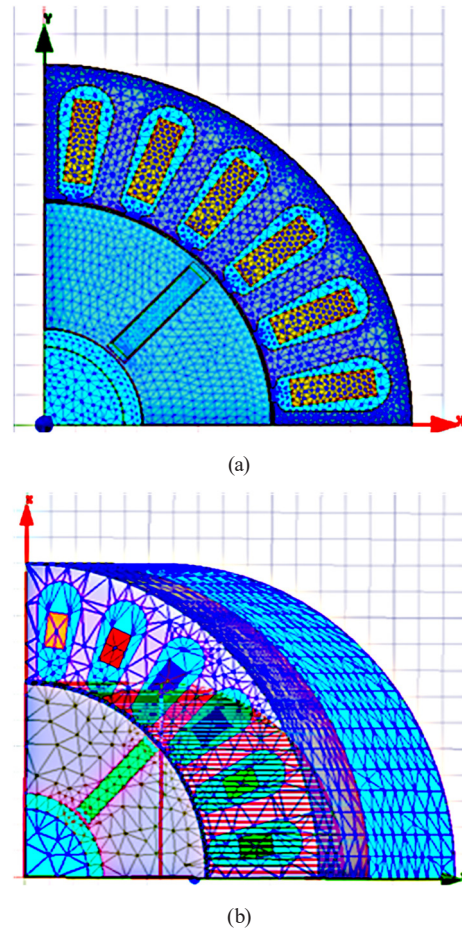
of 65 mm. All electromagnetic performance parameters and characteristics are obtained by using inbuilt FEM in ANSYS tool. Result from 2D and 3D model FEM analysis are demonstrated and evaluated in Section 4.

Basic steps followed for both 2D and 3D model analysis are same. Simulation times with computational storage space for both analyses are different and the same is reported in Tables 4 and 5. The airgap exists between stator and rotor part of motor plays an important role in machine output torque. Magnetic field produced in airgap region depends on stator core soft magnetic material and rotor hard permanent magnet material. These core materials take an important part in field formation. For higher efficiency, higher performance of motor is attracting the use of Silicon Steel or M-grade steel. The number M indicates the core loss content in iron. Two variety (i.e. processed and semi-processed) of laminated steel are used to avoid this loss in silicon steel.

Table 5 Comparison of the simulation time required for materials used in 2D and 3D analysis

| Materials	2D analysis simulation timing (min)	3D analysis simulation timing (min)
Silicon Steel M36	2.25	342.17
Nickel Steel 4750	3.31	169.65
Cobalt Steel Hyperco 50	2.66	190.76
Low Carbon Steel 1020	2.56	140.71
Alloy Powder (Koolmu 90 mu)	2.42	168.45

Mostly Silicon Steel M36 is preferred to avoid free of magnet ageing. But to proof its characteristics in core design, field of motor a comparison purpose is introduced in the study. For this, Nickel Steel 4750, Cobalt Steel Hyperco 50, Low Carbon Steel 1020, and Alloy Powder (Koolmu 90 mu) is considered in the study.

In literature [28] described the importance of Cobalt Steel Hyperco 50, Low Carbon Steel 1020 as a core material for IMs. Here for more clarification, two more materials included for analysis. Therefore, five soft magnetic ferrite-based materials are considered under study. From the data reported in Table 5, it is clear that, the simulation time is not same for the materials under study. Fig. 5 shows the B-H curve of all materials used in simulation for comparative study. As the simulations are done with the 2D and 3D FEM, factors that may affect the parameters like saturation, leakage flux, fringing and relative permeability have been taken into consideration. Here it is observed that saturation point of each material is different.

Silicon Steel M36 has linear characteristics than others. Nickel and cobalt steel have earlier saturation level. Nature of B-H curve observed for each magnetic material changes the characteristics of PMSM designed in the study.
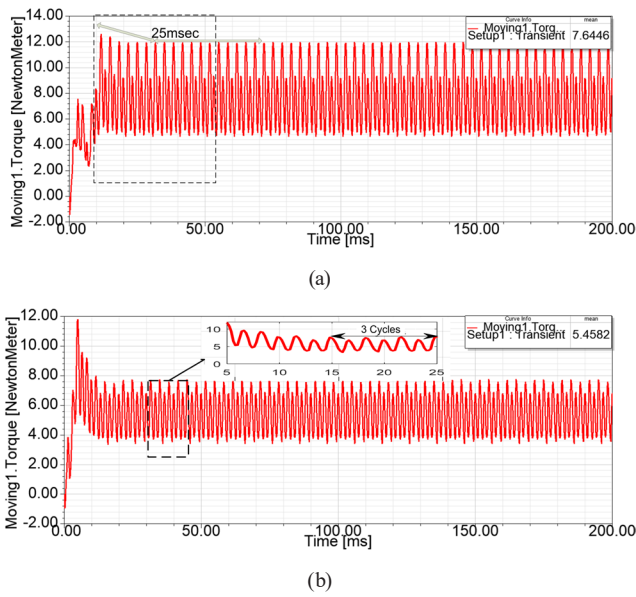
4.1 Torque

Torque under transient condition using magnetic field parameters is calculated for Silicon Steel and its waveforms are illustrated in Fig. 6. Output torque is elaborated in Fig. 6(a) and (b) for 2D and 3D models respectively. From Fig. 6(a), it can be clarified that 2D model-based motor has maximum torque of 12.5851 Nm during starting. It has mean torque of 7.6476 Nm. From the Fig. 6(a), it is observed that the synchronization is reaching at ≈ 25 ms. Similarly, from Fig. 6(b), it can be seen that steady state of motor is achieved 12 ms in advance for 3D model analysis.

(a)

(b)

(c)

(d)

(e)
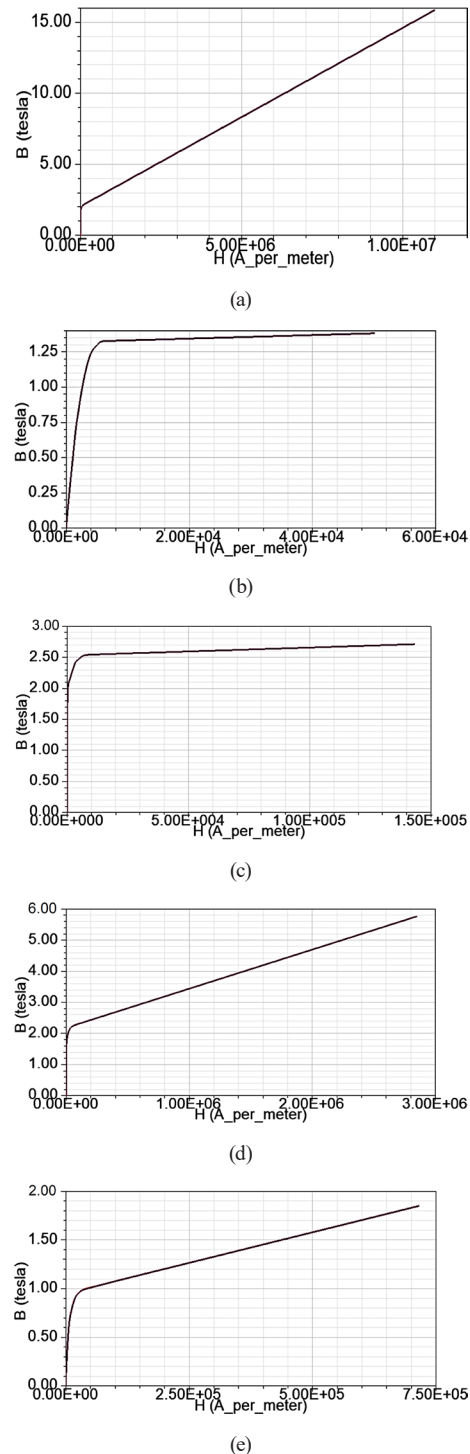
Fig. 5 2D and 3D B-H characteristics of an IPMSM design with (a) Silicon Steel; (b) Nickel Steel; (c) Cobalt Steel Hyperco 50; (d) Low Carbon Steel 1020; (e) Alloy Powder

The mean output and maximum torque at starting obtained in 2D model is 5.4602 Nm and 11.8080 Nm respectively.

From results it is noticed that the average output and maximum torque under 3D model is 28.6% and 6.17% less
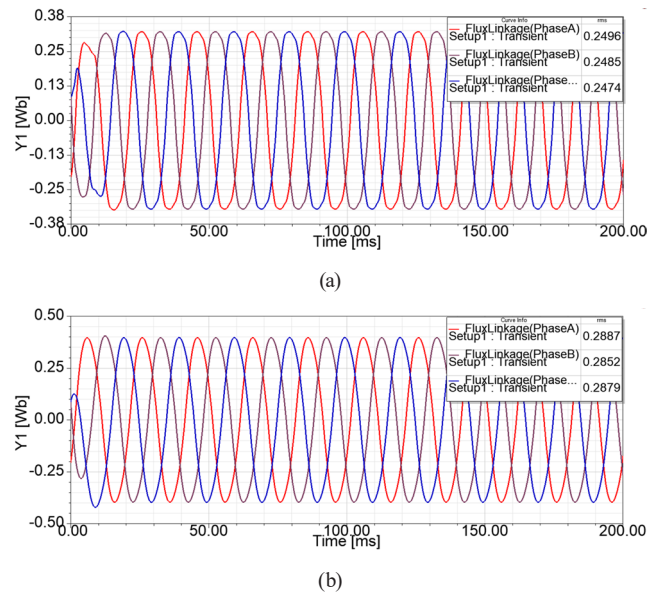
(a)

(b)

Fig. 6 Torque characteristics of a IPMSM with (a) 2D model; (b) 3D model

(a)

(b)

Fig. 7 Flux linkage under transient condition of an IPMSM with
(a) 2D model; (b) 3D model

compared with 2D model FEM analysis. These data related to the torque for different core materials used are reported in Table 6. It also elaborates the changes in output torque for the change of core material with respect to that Silicon Steel M36.From the date reported in Table 6 it is observed that variation in torque is from 3 to 10% difference by different core materials used between 2D and 3D analysis.

4.2 Flux linkages

In IPMSM, flux linkage to stator winding is varying with rotational field which is proportional to strength of PM. Flux linkage has also affected the armature reaction in stator and the two components (one is due to rotor magnetic field, and another is reluctance torque) of electromagnetic torque (T_{em}) performance. Results reported in Fig. 7(a) and (b) are depicts the comparison of flux linkage of three phases A, B, C of stator core to verify paper objective. Fig. 7(a) indicates the results of the flux linkage under 2D model and Fig. 7(b) shows under 3D model. From the Fig. 7(a) and (b), it can be observed that RMS value of flux linkage in case of 2D analysis is lower than that of in 3D which is denoted by variable Y1 in Y axis of the plot.

In 2D analysis, PhaseA RMS value of flux linkage is 0.2496 Wb and in 3D it is 0.2887 Wb. Significant differ-

ence ≈ 0.04 Wb is observed between both analyses. From these results it can be identified that, 3D analysis is required to check the accuracy of flux linkage. The data reported in Table 7 elaborates these difference and variation of flux linkage of stator in 2D and 3D analysis for different core materials used in the study.

From the Table 7, it is found that there is large variation in flux linkage (≈ 34% for 2D, ≈ 25% for 3D analysis) between alloy powder and Silicon Steel M36 used core. Results from the Table 7 depicts that, alloy powder has less flux linkage in both 2D and 3D analysis.

4.3 Stator current

Fig. 8(a) and (b) show the results of the stator current waveforms plotted using 2D and 3D analysis. Fig. 8(a) and (b) help to compare the currents of three phase A, B, C. under transient and steady state.

In the simulation, non-linear properties of the magnetic circuit is considered in ANSYS Maxwell, as a result, the current waveforms in Maxwell 2D and 3D are distinct.

From current waveforms it is clearly visible that RMS value of stator current of phase-a is more in case of 2D compared with 3D analysis. In 2D, current observed is

Table 6 Output torque details under 2D and 3D analysis of a IPMSM under different used core materials

Core material	Output torque in 2D analysis (Nm)	2D variation w.r.t. Silicon Steel M36 (%)	Output torque in 3D analysis (Nm)	3D variation w.r.t. Silicon Steel M36 (%)	2D and 3D deviation (%)
Nickel Steel 4750	12.11	−3.76	10.96	−7.11	−9.44
Cobalt Steel Hyperco 50	10.6	−15.76	11.27	−4.5	6.32
Low Carbon Steel 1020	12.25	−2.61	11.83	0.22	−3.43
Alloy Powder (Koolmu 90 mu)	10.22	18.76	9.32	−21.02	−8.77

Table 7 Flux linkage comparative study of 2D and the 3D analysis of a IPMSM under different used core materials

Core material	Stator flux linkage in 2D analysis (Wb)	2D variation w.r.t. Silicon Steel M36(%)	Stator flux linkage in 3D analysis (Wb)	3D variation w.r.t. Silicon Steel M36 (%)	2D and 3D deviation (%)
Nickel Steel 4750	0.19	−20.59	0.24	−14.27	24.87
Cobalt Steel Hyperco 50	0.28	14.66	0.31	9.31	10.27
Low Carbon Steel 1020	0.26	4.40	0.29	3.08	14.19
Alloy Powder (Koolmu 90 mu)	0.16	−34.13	0.21	24.55	32.48
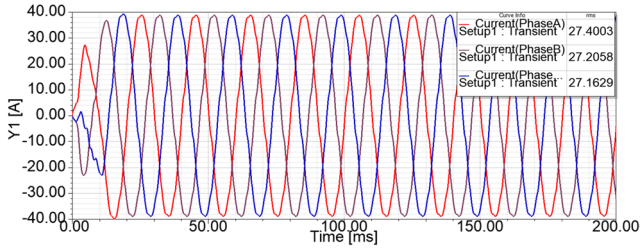
(a)
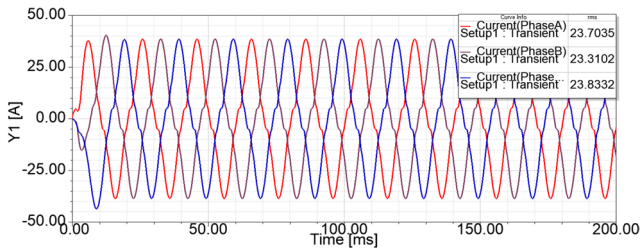
(b)

Fig. 8 Winding current of an IPMSM stator with (a) 2D model; (b) 3D model
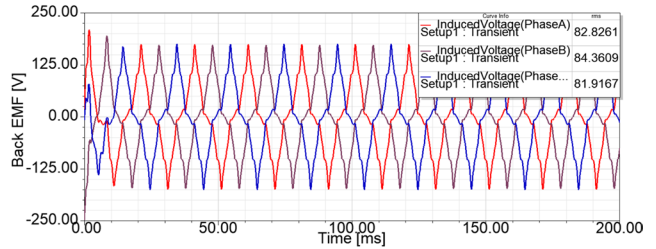

(a)

(b)

Fig. 9 Back EMF of an IPMSM under transient condition with (a) 2D model; (b) 3D model

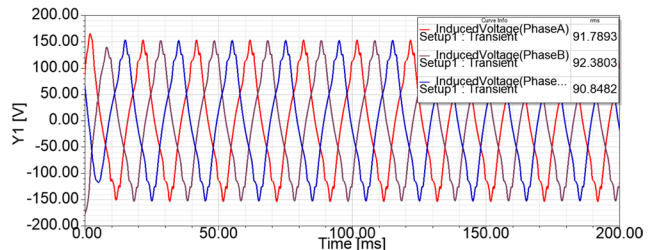27.4003A and in 3D it is 23.7035A under three phase balanced condition.

Under considered materials for core design, deviation observed between 2D, and 3D analyses is greater than 10%. In comparing with Silicon Steel M36, alloy powder has large variation in stator current and it is 31.56% for 2D and 35.24% for 3D analysis. All these results are depicted in Table 8.

4.4 Back EMF

Flux linkage to each phase is varying with rotor position. The phase of the induced EMF can be influenced by the initial position of the rotor, but it cannot modify the amplitude. Back EMF due to flux linkage of phase winding is simulated and its results are reported in Fig. 9(a) and (b) for respective

2D and 3D analysis. PhaseA induced voltage RMS value observed is 82.8261 V under 2D FEM analysis and for the case of 3D, it is 91.7893 V. In 2D and 3D analysis, amplitude of back EMF of each winding is approximately same. This indicates that all three phases are under balanced condition.

All the values of back EMF of IPM motor such as maximum, minimum, peak-peak, average obtained correspond to the 2D and 3D analysis are elaborated in Table 9.

Back EMF of IPM motor obtained by considering different materials for core design is reported in Table 10. From the data reported in Table 10, it is clear that 3.5 to 31% deviation in back EMF is observed between 2D and 3D analysis for core designed with different materials. Core designed using Cobalt Steel Hyperco 50 has less

Table 8 RMS current comparative study of 2D and 3D analysis of a IPMSM under different used core materials

Core material	RMS stator current in 2D analysis (A)	2D variation w.r.t. Silicon steel M36 (%)	RMS stator current in 3D analysis (A)	3D variation w.r.t. Silicon Steel M36 (%)	2D and 3D deviation (%)
Nickel Steel 4750	32.68	19.29	28.45	20.05	−12.94
Cobalt Steel Hyperco 50	23.44	−14.43	20	−15.61	−14.68
Low Carbon Steel 1020	26.23	−4.27	22.65	−4.40	−13.61
Alloy Powder (Koolmu 90 mu)	36.04	31.56	32.05	35.24	−11.06

Table 9 Back EMF of PhaseA IPMSM core designed using Silicon Steel M36

Analysis	Maximum vack EMF (V)	Minimum back EMF (V)	Peak-peak back EMF (V)	Average back EMF (V)
2D	209.6769	−174.7778	383.8778	0.2712
3D	165.7801	−153.5982	319.3783	0.1578

Table 10 Back EMF comparative study of 2D and 3D analysis of a IPMSM under different used core materials

Core material	RMS value of back EMF in 2D analysis (V)	2D variation w.r.t. Silicon Steel M36 (%)	RMS value of back EMF in 3D analysis (V)	3D variation w.r.t. Silicon Steel M36 (%)	2D and 3D deviation (%)
Nickel Steel 4750	64.7	−21.87	78.47	−14.50	21.28
Cobalt Steel Hyperco 50	97.27	17.43	100.72	9.74	3.55
Low Carbon Steel 1020	86.97	5.01	94.68	3.15	8.86
Alloy Powder (Koolmu 90 mu)	52.7	−36.36	68.88	−24.95	30.7

deviation ≈ 3.5 % between 2D and 3D analysis of induced voltage. Also observed is that core designed with Low Carbon Steel 1020 material has less variation (≈ 3%) in induced voltage from use of Silicon Steel M36.
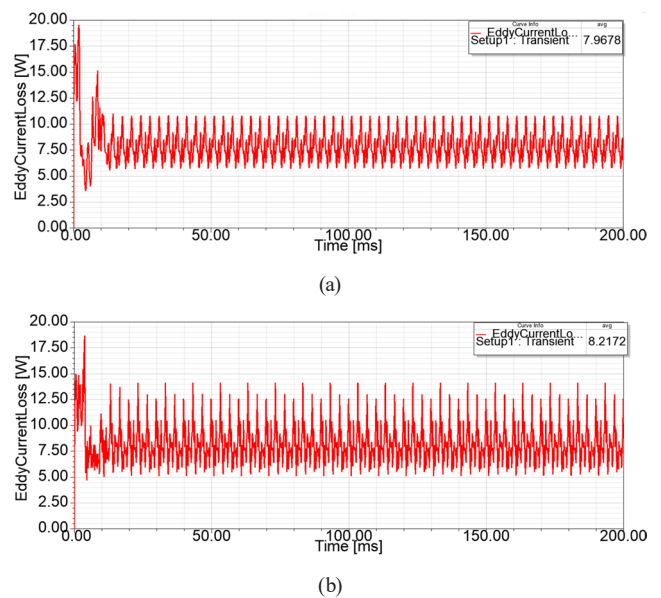
4.5 Eddy-current losses

Rare-earth permanent magnets used in IPMSM have higher conductivity than an electromagnet. With the increasing use of high conductivity magnets, the loss of eddy current in a magnet is another issue that needs to focus. Eddy-current loss in the magnets is particularly high in an IPMSM with concentrated windings. The Eddy-current generated in the PMs is the reason behind demagnetization with heating effect in addition to losses of motor [29]. The Eddy-current losses arising in the conductive material is expressed in Eq. (15):

$$P_{\text{Eddy}} = \iint_{\Omega_c} \frac{|J_{\text{Eddy}}|^2}{\sigma} dx \, dy. \tag{15}$$

Here corresponds to the Eddy-current losses in a conductive region Ω_c, σ is the conductivity and J_{Eddy} is the Eddy-current density induced in conductive domain.

Simulated results of eddy current losses of IPM motor using Eq. (15) are shown in Fig. 10. Eddy-current loss characteristic under 2D and 3D analysis is separately reported in Fig. 10(a) and (b) respectively. From the results it is observed that, 3D analysis is giving more eddy current loss and its average is 8.2172 W. For 2D analysis, the average is around 7.9678 W. Eddy-current plot of 3D analysis gives additional detail about the distortion in the eddy current losses, especially during the first 5 msec.

Data reported in Table 11 describes Eddy-current losses with different materials used for core design and their variation with respect to Silicon Steel M36. From the Table 11 it is observed that, Low Carbon Steel 1020

**Fig. 10** Eddy-current loss of an IPMSM with (a) 2D model; (b) 3D model

has highest eddy current loss for 2D it is ≈ 23 W and for 3D analysis it is ≈ 20 W. Other three materials have low eddy current loss as compared to that of Silicon Steel M36. Through the eddy current loss simulation for Nickel Steel 4750 core, deviation observed between 2D and 3D analysis is 76.42% and for alloy powder, the deviation observed is 2.08%. These results help to understand the importance of 3D analysis especially for designing an IPMSM.

4.6 Magnetic flux density

Under magneto static condition, Maxwell 2D and 3D are used to determine magnetic flux density (B) of spoke shape IPM motor. Importance of B analysis is discussed in Section 2 here, comparison of both analyses and its results are discussed. Contour plot of flux density for 2D and 3D are demonstrated in Fig. 11. The section along PM in stator core is highly saturated as shown in Fig. 11 indicates

Table 11 Eddy-current loss comparative study of 2D and 3D analysis of an IPMSM under different used core materials

Core material	Average Eddy-current loss in 2D analysis (W)	2D variation w.r.t. Silicon Steel M36 (%)	Average Eddy-current losses in 3D analysis (W)	3D variation w.r.t. Silicon Steel M36 (%)	2D and 3D deviation (%)
Nickel Steel 4750	3.64	−54.31	6.43	−21.69	76.42
Cobalt Steel Hyperco 50	2.38	−70.08	2.49	−69.65	4.63
Low Carbon Steel 1020	21.95	175.57	20.36	147.84	−7.24
Alloy Powder (Koolmu 90 mu)	2.86	−64.1	2.80	−65.91	−2.08

(a)

(b)
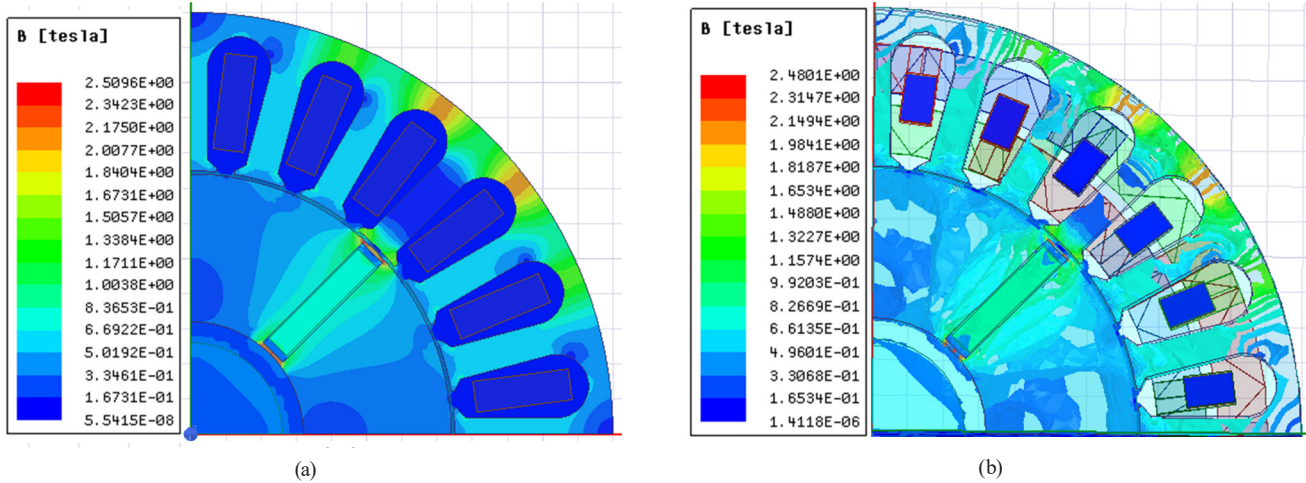
Fig. 11 Magnetic flux density distribution of IPMSM with (a) 2D model; (b) 3D model

that; these regions are sensitive toward armature reaction. From Fig. 11, it is observed that; the magnetic flux density of the IPM motor is 2.5098T in 2D analysis, and the same IPM motor under 3D is 2.4801 T. From the analysis, there is a significant difference is observed between 2D and 3D analysis of the magnetic field. This is due to motor end windings and skewing of stator slots. For understanding more about this, the analysis is extended with the change of materials for core design, and its results are reported in Table 12. Under 2D analysis, Silicon Steel M36 has equal magnetic flux density as that of Alloy powder unlike in 3D analysis. Under 3D analysis Low Carbon Steel 1020 has less variation with Silicon Steel M36. Percentage deviation between 2D and 3D analysis is minimum ≈ 3% for the core designed with cobalt steel Hyperco 50.

4.7 Airgap flux density

The results of air-gap flux density distribution for 2D and 3D analysis is plotted in Fig. 12. A 4-pole motor is taken for the analysis and flux density distribution in airgap under each pole is represented by Fig. 12. The difference in air-gap flux density distribution between 2D and 3D studies is quite modest. From the Fig. 12 it is seen that, 3D analysis is provided distorted plot as compared with 2D indicates 3D analysis is more suitable for system depth investigation.

For 2D analysis, the average value of B_{airgap} is 0.3388 T and for 3D, it is 0.3455 T. This means that the 2D analysis' outcomes are satisfactory. For more analysis, radial component of airgap magnetic flux density is also considered for comparative study which is given in Fig. 13. In this case also, difference between the radial B_{airgap} in 2D and

Table 12 Magnetic flux density comparative study of 2D and 3D analysis of an IPMSM under different used core materials

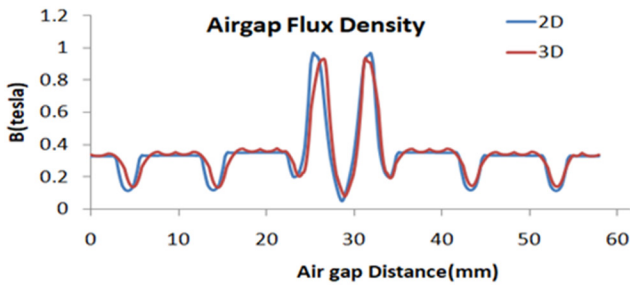| Core material	Magnetic flux density in 2D analysis (Tesla)	2D variation w.r.t. Silicon Steel M36 (%)	Magnetic flux density in 3D analysis (Tesla)	3D variation w.r.t. Silicon Steel M36 (%)	2D and 3D deviation (%)
Nickel Steel 4750	1.8	−28.25	1.93	−22.05	7.35
Cobalt Steel Hyperco 50	2.93	16.9	2.84	14.77	−2.98
Low Carbon Steel 1020	2.24	−10.37	2.6	4.92	15.68
Alloy Powder (Koolmu 90 mu)	2.50	−0.07	1.48	−40	−40.7

Fig. 12 Comparison of the air-gap flux density distribution of IPMSM between 2D and 3D analysis
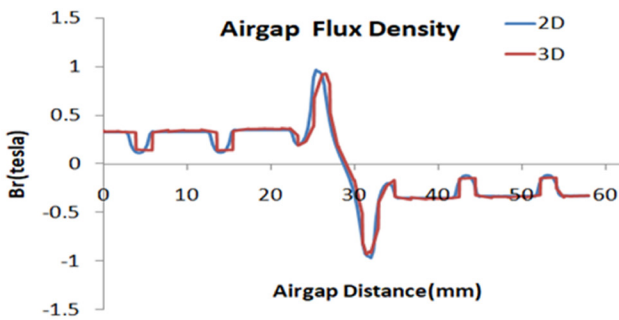

Fig. 13 Comparison of the radial component of airgap flux density distribution of IPMSM between 2D and 3D analysis

3D analysis is less. Also, it observed that the 2D analysis gives an earlier response for reaching maximum B_{airgap} compared with 3D.

Table 13 provides additional data regarding airgap flux density comparative study.

It is shown that core designed using Alloy Powder has large deviation between 2D and 3D analysis of airgap flux density. Difference between airgap flux density of Alloy Powder and Silicon Steel M36 is less (≈ 1.3 %) compared to others core materials in 2D analysis. In 3D analysis, Low Carbon Steel 1020 has less difference of airgap flux density from Silicon Steel M36.

Each case of parameters considered for 2D and 3D FEM analysis gives different values. These deviations are due to the changes in the number of meshing elements in 2D and 3D models of the IPM motor. In case of 2D analysis, it is not possible to analyze each part of the IPM motor model from all directions. It only shows surface values of

each parameter of the IPM motor. But in case of 3D analysis, it is possible to deal with each part of the motors like realistic conditions. It is also observed that the linearity is less in the case of 3D analysis. Distortion is also found more in each parameter of the IPM motor in 3D analysis.

5 Conclusion

A variety of ferromagnetic materials were investigated for the design of stator and rotor core. The resulting data was post processed and compared to each other in order to pinpoint the originating inaccuracy, as well as its significance and impact on other calculations. From the results of the study, both 2D and 3D provide an accurate solution for design of IPM motor. In torque characteristics, 2D analysis has shown a better performance. Deviation in toque observed between 2D and 3D, is 2.1864 Nm. But in case of flux linkage, 3D analysis provides an enhanced solution. Other parameters like airgap flux density, back EMF, stator current of IPM motor, magnetic flux density is also properly analyzed in 2D and 3D analysis. For preliminary study of the motor, 2D analysis is more appropriate while 3D analysis provides a detail clarification about the motor. So that the measured value of performance parameters is differed in both cases. Result accuracy is same which is clearly visible from airgap flux density with radial components comparison where 3D result has 1.9% deviation with respect to 2D. Also, in case of surface magnetic flux density 1.1% difference is observed between 2D and 3D result. Number of meshing elements in 3D FEM analysis has greater and leads to more simulation time. This reason is encouraging to follow 2D analysis for IPM motor design. Core Steel M36 performance is compared with other four materials to show its effect on electromagnetic and electromechanical quantities. Deviation in the parameters and errors, after use of these materials has shown the importance of M36 for stator and rotor design. It is giving better results and economically suitable compared with other materials under study.

Table 13 Airgap flux density comparative study of 2D and the 3D analysis of an IPMSM under different used core materials

Core material	Airgap flux density in 2D analysis (Tesla)	2D variation w.r.t. Silicon steel M36 (%)	Airgap flux density in 3D analysis (Tesla)	3D Variation w.r.t. Silicon Steel M36 (%)	2D and 3D deviation (%)
Nickel Steel 4750	0.2911	−14.07	0.2924	−15.36	0.44
Cobalt Steel Hyperco 50	0.3675	8.47	0.3670	6.22	−0.13
Low Carbon Steel 1020	0.3289	−2.92	0.3452	−0.08	4.95
Alloy Powder (Koolmu 90 mu)	0.3344	−1.29	0.2464	−28.68	26.31

References

[1] Sayed, E., Abdalmagid, M., Pietrini, G., Sa'adeh, N.-M., Dorneles Callegaro, A., Goldstein, C., Emadi, A. "Review of Electric Machines in More-/Hybrid-/Turbo-Electric Aircraft", IEEE Transactions on Transportation Electrification, 7(4), pp. 2976–3005, 2021.
https://doi.org/10.1109/TTE.2021.3089605

[2] Agrawal, J., Bodkhe, S. "Steady-state analysis and comparison of control strategies for PMSM", Modelling and Simulation in Engineering, 2015, 306787, 2015.
https://doi.org/10.1155/2015/306787

[3] Mishra, A., Agarwal, P., Srivastava, S. P. "A comprehensive analysis and implementation of vector control of permanent magnet synchronous motor", International Journal of Power and Energy Conversion, 5(1), pp. 1–23, 2014.
https://doi.org/10.1504/IJPEC.2014.059982

[4] Hwang, C. C., Chang, C. M., Cheng, S. P., Chan, C. K., Pan, C. T., Chang, T. Y. "Comparison of performances between IPM and SPM motors with rotor eccentricity", Journal of Magnetism and Magnetic Materials, 282, pp. 360–363, 2004.
https://doi.org/10.1016/j.jmmm.2004.04.084

[5] Ou, J., Liu, Y., Doppelbauer, M. "Comparison study of a surface-mounted PM rotor and an interior PM rotor made from amorphous metal of high-speed motors", IEEE Transactions on Industrial Electronics, 68(10), pp. 9148–9159, 2020.
https://doi.org/10.1109/TIE.2020.3026305

[6] Mukherjee, P., Paitandi, S., Sengupta, M. "Comparative analytical and experimental study of fabricated identical surface and interior permanent magnet BLDC motor prototypes", Sādhanā, 45(1), 26, 2020.
https://doi.org/10.1007/s12046-019-1264-0

[7] Sun, H., Chen, Y., Ma, C., Moghaddam, A. F., Sergeant, P., Van den Bossche, A. "A novel design and electromagnetic analysis for a linear switched reluctance motor", Electrical Engineering, 101(2), pp. 609–618, 2019.
https://doi.org/10.1007/s00202-019-00812-x

[8] Torres, J., Moreno-Torres, P., Navarro, G., Blanco, M., Nájera, J., Santos-Herran, M., Lafoz, M. "Asymmetrical Rotor Skewing Optimization in Switched Reluctance Machines Using Differential Evolutionary Algorithm", Energies, 14(11), 3194, 2021.
https://doi.org/10.3390/en14113194

[9] Tosun, N., Ceylan, D., Polat, H., Keysan, O. "A comparison of velocity skin effect modeling with 2-D transient and 3-D quasi-transient finite element methods", IEEE Transactions on Plasma Science, 49(4), pp. 1500–1507, 2021.
https://doi.org/10.1109/TPS.2021.3067105

[10] Diab, H., Amara, Y., Barakat, G., Ghandour, M. "Translator Eccentricity Analysis in Tubular Linear Machines Using Quasi-3-D Finite Element Method Modeling", IEEE Transactions on Magnetics, 58(2), 8101105, 2022.
https://doi.org/10.1109/TMAG.2021.3078399

[11] Bouheraoua, M., Atig, M., Bousbaine, A., Benamrouche, N. "Electro-Thermal Coupled Modeling of Induction Motor Using 2D Finite Element Method", Advances in Electrical and Computer Engineering, 21(2), pp. 33–40, 2021.
https://doi.org/10.4316/AECE.2021.02004

[12] Pechlivanidou, M. C., Chasiotis, I. D., Karnavas, Y. L. "A comparative study on 2D and 3D magnetic field analysis of permanent magnet synchronous motor using FEM simulations", Journal of Electromagnetic Waves and Applications, 33(17), pp. 2215–2241, 2019.
https://doi.org/10.1080/09205071.2019.1674190

[13] Dalcali, A., Akbaba, M. "Comparison of 2D and 3D magnetic field analysis of single-phase shaded pole induction motors", Engineering Science and Technology, an International Journal, 19(1), pp. 1–7, 2016.
https://doi.org/10.1016/j.jestch.2015.04.013

[14] Hong, C., Huang, W., Hu, Z. "Design and analysis of a high-speed dual stator slotted solid-rotor axial-flux induction motor", IEEE Transactions on Transportation Electrification, 5(1), pp. 71–79, 2019.
https://doi.org/10.1109/TTE.2018.2880301

[15] Dmitrievskii, V., Prakht, V., Anuchin, A., Kazakbaev, V. "Traction synchronous homopolar motor: simplified computation technique and experimental validation", IEEE Access, 8, pp. 185112–185120, 2020.
https://doi.org/10.1109/ACCESS.2020.3029740

[16] Ferkova, Z. "Comparison between 2D and 3D modelling of induction machine using finite element method", Advances in Electrical and Electronic Engineering, 13(2), pp. 120–126, 2015.
https://doi.org/10.15598/aeee.v13i2.1346

[17] Li, B., Zhao, J., Mou, Q., Liu, X., Haddad, A., Liang, J. "Research on torque characteristics of a modular arc-linear flux switching permanent-magnet motor", IEEE Access, 7, pp. 57312–57320, 2019.
https://doi.org/10.1109/ACCESS.2019.2913952

[18] Torkaman, H., Afjei, E. "Comprehensive Study of 2-D and 3-D Finite Element Analysis of a switched reluctance motor", Journal of Applied Sciences, 8(15), pp. 2758–2763, 2008.
https://doi.org/10.3923/jas.2008.2758.2763

[19] Bianchi, N., Bolognani, S., Carraro, E., Castiello, M., Fornasiero, E. "Electric vehicle traction based on synchronous reluctance motors", IEEE Transactions on Industry Applications, 52(6), pp. 4762–4769, 2016.
https://doi.org/10.1109/TIA.2016.2599850

[20] Breban, S., Dranca, M., Chirca, M., Pacuraru, A.-M., Teodosescu, P.-D., Oprea, C.-A. "Experimental Tests on a Spoke-Type Permanent Magnets Synchronous Machine for Light Electric Vehicle Application", Applied Sciences, 12(6), 3019, 2022.
https://doi.org/10.3390/app12063019

[21] Gupta, C., Marwaha, S., Manna, M. S. "Finite element method as an aid to machine design: A computational tool", In: Proceedings of the COMSOL Conference, Bangalore, India, 2009, pp. 1–6. ISBN 9780982569726 [online] Available at: https://www.comsol.com/paper/download/46260/Gupta.pdf [Accessed: 15 July 2022]

[22] Yoon, K.-Y., Hwang, K.-Y. "Optimal design of spoke-type IPM motor allowing irreversible demagnetization to minimize PM weight", IEEE Access, 9, pp. 65721–65729, 2021.
https://doi.org/10.1109/ACCESS.2021.3070747

[23] Naik, S., Bag, B., Chandrasekaran, K. "Comparative Analysis of Surface Mounted and Interior Permanent Magnet Synchronous Motor for Low rating Power Application", Journal of Physics: Conference Series, 2070, 012119, 2021.
https://doi.org/10.1088/1742-6596/2070/1/012119

[24] Xiao, Y., Zhu, Z. Q., Jewell, G. W., Chen, J., Wu, D., Gong, L. "A novel spoke-type asymmetric rotor interior permanent magnet machine", IEEE Transactions on Industry Applications, 57(5), pp. 4840–4851, 2021.
https://doi.org/10.1109/TIA.2021.3099452

[25] Song, J.-Y., Lee, J.-H., Kim, Y.-J., Jung, S.-Y. "Computational method of effective remanence flux density to consider PM overhang effect for spoke-type PM motor with 2-D analysis using magnetic energy", IEEE Transactions on Magnetics, 52(3), 8200304, 2016.
https://doi.org/10.1109/TMAG.2015.2475266

[26] Belay Muna, Y., Kuo, C.-C. "Magnetic field distribution of magnetic encoder with TMR sensor using finite element analysis", Microsystem Technologies, 26(8), pp. 2683–2701, 2020.
https://doi.org/10.1007/s00542-020-04812-x

[27] ANSYS, Inc. "ANSYS, (2018.1)" [computer program], Available at: https://www.ansys.com [Accessed: 10 July 2022]

[28] Yassin, Y. A., Hussain, A. N., Ahmed, N. Y. "Comparison and assessment of a different steel materials based on core losses reduction for three-phase induction motor", International Journal of Power Electronics & Drives Systems (IJPEDS), 12(1), pp. 51–62, 2021.
https://doi.org/10.11591/ijpeds.v12.i1.ppxx-yy

[29] Oh, S. Y., Cho, S.-Y., Han, J.-H., Lee, H. J., Ryu, G.-H., Kang, D., Lee, J. "Design of IPMSM rotor shape for magnet Eddy-current loss reduction", IEEE Transactions on Magnetics, 50(2), 7020804, 2014.
https://doi.org/10.1109/TMAG.2013.2282473